Vibrational Absorption and Circular Dichroism Studies of *trans*-(3*S*,4*S*)-d_6-Cyclopentene in the Gas Phase

Dominique Cavagnat,* Laure Lespade, and Thierry Buffeteau

Institut des Sciences Moléculaires, UMR 5255 - CNRS, Université de Bordeaux I, 351 cours de la Libération, 33405 Talence, France

Received: March 21, 2007; In Final Form: May 2, 2007

Vibrational absorption (IR) and circular dichroism (VCD) measurements of *trans*-(3*S*,4*S*)-d_6-cyclopentene in the gas phase were performed in the C−H, C−D, and mid-infrared regions. In this study, we report the first VCD spectra recorded at high spectral resolution (up to 0.5 cm^{-1}) with a very good signal-to-noise ratio (differential absorbance lower than 5×10^{-6}). The quality of the experimental spectra allows us the observation of the vibration−rotation structure of the bands in both absorption and VCD spectra. Experimental spectra have been compared with the density functional theory (DFT) absorption and VCD spectra, calculated using B3LYP functional and cc-pVTZ basis set for the axial, equatorial, and planar conformers. Lorentzian and PQR band profiles have been used to convert the calculated dipolar and rotational strengths. In the mid-infrared (<2000 cm^{-1}) region, predicted (population-weighted) spectra were in excellent agreement with experiment, allowing the determination of the absolute configuration of this molecule. Above 2000 cm^{-1}, a reasonable agreement was obtained even if anharmonicity was not considered and if Fermi resonance occurs in the C−D stretching region. Finally, a more precise analysis of the absorption spectrum has been achieved by taking into account anharmonicity of the C−H stretching and its coupling with the ring-puckering motion.

1. Introduction

Vibrational circular dichroism (VCD) is the differential absorption by chiral molecules of left- and right-handed circularly polarized radiation in the infrared (IR) region.[1] During past decade, VCD appeared as a very promising tool for the study of the conformational analysis of chiral organic compounds.[2] Indeed, the VCD spectrum of a chiral molecule depends on its absolute configuration but also, in the case of flexible molecules, on its conformation. The relation between the VCD spectrum and the structure of a chiral molecule can be rationalized from quantum mechanical calculations.[3] By comparing the experimental spectrum with the calculated spectrum of one enantiomer with a given conformation, it is possible to identify the absolute configuration and the conformation of a chiral molecule.

Most of the VCD studies have been performed with compounds in solution, but VCD spectra can also be realized in the gas phase. This physical state presents the advantage that molecules are isolated (i.e., no intermolecular interaction with solvent) and that VCD spectra are not perturbed by solvent absorption. In return, the compounds must have a relatively high vapor pressure at room temperature. So far, only few gas-phase VCD studies have been performed for small rings made optically active by isotopic substitution.[4−6] In the earlier papers reported for *trans*-(1*R*,2*R*)-dideuteriocyclobutane,[4] the experimental absorption and VCD spectra were recorded in the C−H and C−D stretching region and in the mid-IR range on a dispersive VCD instrument at relatively low resolution (from 12 to 4 cm^{-1}). The principal aim of these studies was the comparison of the two calculation models formulated at that time (i.e., the fixed partial charge (FPC) model[7] and the localized molecular orbital (LMO) model[8]) in view to reproduce the experimental VCD spectrum of this molecule. A better agreement between calculated and experimental results was found for the FPC model. The effect of the puckering motion of cyclobutane was not analyzed because the absorption and VCD spectra were recorded at low resolution. All the other gas-phase studies deal with derivatives of cyclopropane, a smaller rigid cycle. The absorption and VCD spectra of gaseous *trans*-(1*S*,2*S*)-dideuteriocyclopropane[5] were recorded in the mid-IR on a FTIR spectrometer at a better resolution (1 cm^{-1}). At this resolution, the VCD bands exhibit the same vibration−rotation contours as those observed for the absorption bands. Finally, the two following papers[6] about (2*S*,3*S*)-1-^{13}C-1,2,3-d_3 cyclopropane investigated the optical activity arising from ^{13}C substitution.

In this paper, we present an IR and VCD gas phase study of a derivative of cyclopentene made optically active by selective deuteriation, the *trans*-(3*S*,4*S*)-d_6-cyclopentene, **1**. The conformational flexibility of cyclopentene which interconverts via a puckering motion between two equivalent nonplanar ring structures (Figure 1) has been the subject of a great number of experimental[9,10] and theoretical[11] investigations. They have evidenced that the puckering potential $V(x)$ (x being the puckering coordinate) can be modeled by a polynomial form and that it has a double minimum with a barrier to planarity of about 230 cm^{-1}. Furthermore, the coupling between the ring-puckering motion and the other vibrations has been extensively studied in particular in the C−H stretching region.[10,12,13] The VCD analysis of **1** completes the previous experimental and theoretical spectroscopic studies. In particular, the presence of vibration−rotation structures, previously observed in the high resolution absorption and VCD spectra of small rigid cyclopropane derivative,[5] can be analyzed in the case of this larger flexible molecule. Moreover, the effect of the ring-puckering motion on the VCD spectrum can be investigated in particular

* Corresponding author. Fax: 335 4000 8402. E-mail: d.cavagnat@ism.u-bordeaux1.fr.

10.1021/jp0722556 CCC: $37.00
Published on Web 07/06/2007

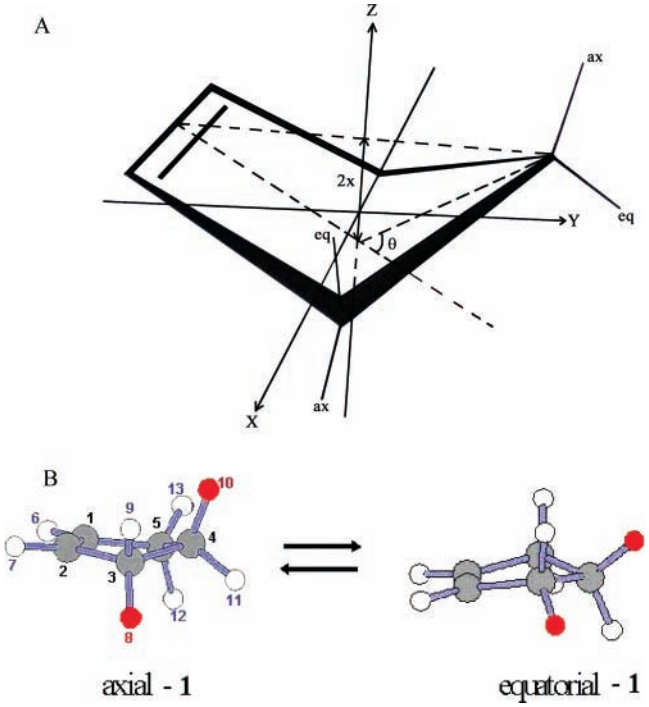

Figure 1. (A) Puckered equilibrium conformation of the cyclopentene molecule and definition of the ring-puckering coordinate x ($22° < \theta < 26°$). (B) The two equilibrium axial and equatorial conformers and atomic numbering of *trans*-(3*S*,4*S*)-d_6-cyclopentene **1** (H, red circles; D, white circles; C, gray circles).

in the C−H stretching region where the coupling between these vibrations has been precisely observed and modeled for the absorption spectrum.

The structure of the paper will be as follows: after the presentation of the experimental procedure for the synthesis and the spectrum measurements, the methods used for the spectra calculations are briefly recalled. In the last part, the experimental spectra are compared with the calculated ones and discussed.

2. Experimental Section

Synthesis. The (2*S*,3*S*)-1,4-dibromo-2,3-dideuteriobutane was obtained following the synthetic route previously reported in the literature.[14] Cyclization of this compound in ether solution in presence of magnesium and CO_2 led to 3,4-d_2-cyclopentanone which was further deuterated by exchange in D_2O to give 2,2,3,4,5,5-d_6-cyclopentanone. The *trans*-(3*S*,4*S*)-d_6-cyclopentene, **1**, was obtained by first treating the d_6-cyclopentanone with tosylhydrazine and then the formed diazo compound with alkyl lithium in ether solution. The isotopic purity, as checked by mass spectrometry, is higher than 96%.[15] The *trans*-(3*S*,4*S*)-d_6-cyclopentene was then dried with sodium filaments, degassed by the freeze-pump thaw method, and transferred under vacuum into a gas cell.

Measurements of the IR and VCD Spectra. The IR and VCD spectra were recorded with a ThermoNicolet Nexus 670 FTIR spectrometer equipped with a VCD optical bench.[16] In this optical bench, the light beam was focused on the sample by a BaF_2 lens (191 mm focal length), passing an optical filter (depending on the studied spectral range), a BaF_2 wire grid polarizer (Specac), and a ZnSe photoelastic modulator (Hinds Instruments, Type II/ZS50). The light was then focused by a ZnSe lens (38.1 mm focal length) onto a 1×1 mm^2 HgCdTe (ThermoNicolet, MCTA* E6032) detector. The absorption spectrum of **1** in the gas phase was recorded at a resolution of 0.5 cm^{-1}, by coadding 200 scans. VCD spectra of **1** were

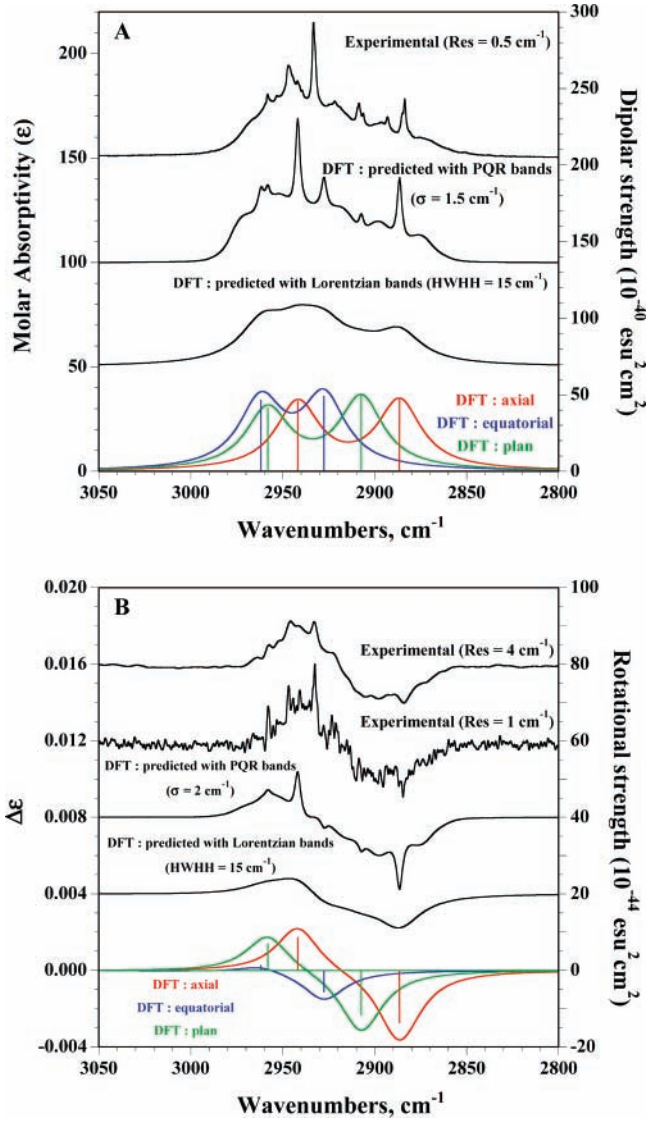

Figure 2. (A) Comparison of the experimental absorption spectrum of *trans*-(3*S*,4*S*)-d_6-cyclopentene in the gas phase (3.2 kPa, 100 mm path length, 0.5 cm^{-1} resolution; higher trace) with calculated absorption spectra in the 3050−2800 cm^{-1} region (lower trace, individual axial, equatorial, and planar conformer spectra; middle trace, predicted spectrum with Lorentzian profiles (15 cm^{-1} HWHH); upper trace, predicted spectrum with vibration−rotation PQR transitions convoluted with Lorentzian profile (1.5 cm^{-1} HWHH)). (B) Comparison of the experimental VCD spectra of *trans*-(3*S*,4*S*)-d_6-cyclopentene in the gas phase (3.2 kPa, 100 mm path length, 1 and 4 cm^{-1} resolution; higher traces) with calculated VCD spectra in the 3050−2800 cm^{-1} region (lower trace, individual axial, equatorial, and planar conformer spectra; middle trace, predicted spectrum with Lorentzian profiles (15 cm^{-1} HWHH); upper trace, predicted spectrum with vibration−rotation PQR transitions convoluted with Lorentzian profile (2 cm^{-1} HWHH)). The frequencies of the DFT spectra calculated at the B3LYP/cc-pVTZ level were scaled by 0.962.

recorded at a medium (4 cm^{-1}) and higher resolution (1 or 0.5 cm^{-1}), by coadding 24 000 scans (8 h acquisition time). A special Pyrex cell for gas-phase experiments was used with 100 mm path length and CaF_2 windows. The cell was filled at room-temperature vapor pressure (50.7 kPa) for the 1700−1000 cm^{-1} spectral range and with lower pressure (≈3.2 kPa) for C−H and C−D stretching regions. Baseline corrections of the VCD spectra were performed by subtracting the VCD spectra of the racemic sample of **1**. The photoelastic modulator was adjusted for a maximum efficiency at 1300, 2200, and 3200 cm^{-1} for experiments in the mid-IR, C−D, and C−H stretching regions,

TABLE 1: Conformations and Energies of Cyclopentene 1

conformer	electronic energy (hartree)	Gibbs energy (hartree)	ΔG^a (cm^{-1})	population[b] (%)
axial	−195.399617941	−195.330915	0	0.431
equatorial	−195.399617941	−195.330900	3.3	0.424
planar	−195.399254841	−195.329899	223.2	0.144

[a] Relative Gibbs energy difference. [b] Population based on Gibbs energies.

respectively. Calculations were performed via the standard ThermoNicolet software, using Happ and Genzel apodization, de-Haseth phase-correction, and a zero-filling factor of 1. Calibration spectra were recorded at the same spectral resolution (4, 1, and 0.5 cm^{-1}) using a birefringent plate (CdSe) and a second BaF_2 wire grid polarizer, following the experimental procedure previously published.[17]

3. Spectra Calculations

Calculation of the VCD and Absorption Spectra. The geometry optimizations, vibrational frequencies, and absorption and VCD intensities were calculated by the Gaussian 03 program (Gaussian, Inc.)[18] on four processors on a SGI ALTIX3300. Calculations of the optimized geometry for the axial, equatorial, and planar conformers of **1** were performed at the density functional theory (DFT) level using B3LYP functional and cc-pVTZ basis set. Vibrational frequencies as well as IR and VCD intensities were calculated at the same level of theory, utilizing the magnetic field perturbation method with gauge invariant atomic orbitals.[19] For comparison to experiment, the calculated frequencies were scaled by 0.962, 0.973, and 0.98 for the C−H, C−D, and mid-IR spectral ranges, respectively.

The dipolar and rotational strengths were represented by vertical lines. They were also converted to Lorentzian bands with 15 cm^{-1} half-width at half-height (HWHH). In addition, to better reproduce the experimental features, they were converted to vibration−rotation PQR profiles. Indeed, cyclopentene is an asymmetrical top molecule ($I_x = 140.6 \times 10^{-40}$ g cm^2, $I_y = 146.2 \times 10^{-40}$ g cm^2, and $I_z = 259.4 \times 10^{-40}$ g cm^2 for **1**). In gas phase, the IR spectra of this type of molecule show typically PQR profiles characterizing the coupling of the vibrations with rotation. Furthermore, according to the μ_x, μ_y, or μ_z components of the dipole moment involved in the given vibration, these profiles have different "A", "B", or "C" type contours, respectively, which have been well described in the literature.[20] For **1**, the "B type" contour is characterized by two sharp Q branches on either side of the zero-line and broader P and R wings ($\Delta PR = 19$ cm^{-1}). The "A" and "C type" contours have a PQR profile with a more or less intense Q branch ("A type", $\Delta PR = 19$ cm^{-1}, Q branch relative intensity = 10%; "C type", $\Delta PR = 27$ cm^{-1}, Q branch relative intensity = 40%). The vibration−rotation transitions have been calculated by Perrin[21] and convoluted with a Lorentzian profile (HWHH = 1−2 cm^{-1}) to obtain the "A", "B", or "C" type contours.

Coupling of the C−H Stretching with the Ring-Puckering Motion. The theoretical approach used to reproduce the ν(C−H) profile has been extensively described in previous papers.[10b,c,12,13] The basic idea of this theory is to suppose that the C−H stretching vibrations of cyclopentene are perturbed by two main couplings: the coupling with the puckering motion and the Fermi resonance couplings involving mostly the deformation modes of the angles adjacent to the considered C−H bond. The ring-puckering motion being slower than the other considered motions, the total Hamiltonian can be solved in the adiabatic approximation and written as the sum of two Hamiltonians:

$$H_T(x,q) = H_{q,p}(x,q) + H_p(x) \quad (1)$$

$H_p(x)$ describing the ring-puckering motion can be written as

$$-\frac{\hbar^2}{2}\left(\frac{\partial}{\partial x}\right)g(x)\left(\frac{\partial}{\partial x}\right)\Psi_n(x) + V_{eff}^{\upsilon}(x)\Psi_n(x) = E_n^{\upsilon}\Psi_n(x) \quad (2)$$

where x is the ring-puckering coordinate.

$g(x)$ is the inverse of the reduced mass of the motion; it is calculated by using the basis bisector model of Malloy[11c] and fitted by a polynomial form of order 6.

V_{eff}^{υ} is the ring-puckering effective potential in the υ vibrational state. In the ground vibrational state, V_{eff}^{0} is the sum of the ring-puckering potential and of the zero-point vibrational energy. In the first excited C−H stretching state, it is increased by the C−H stretching vibrational energy variation

$$V_{eff}^{1}(x) = hc\omega_n(x) + V_{eff}^{0}(x) \quad (3)$$

This energy variation $hc\omega_n(x)$ is obtained by the resolution of the vibrational Hamiltonian $H_{q,p}(x,q)$, which has been extensively described in previous papers.[10b,c,12,13]

The reconstruction of the vibrational spectrum is achieved in two steps. First, the diagonalization of the vibrational Schrödinger equation is completed for different values of the ring-puckering coordinate x (between −0.3 Å and 0.3 Å by step of 0.01 Å) to obtain $hc\omega_n(x)$, the vibrational energy variation. Then, the Schrödinger eq 2 is diagonalized on a basis set of 80 harmonic oscillators for the ground vibrational state $\upsilon = 0$ and the first excited C−H stretching state $\upsilon = 1$. This gives the E_n^0 and E_n^1 energy levels as well as the wave functions $\Psi_n(x)$ corresponding to the state $|0, n\rangle$ and $|1, n\rangle$. The fundamental C−H stretching spectrum is the sum of all the transitions between the ring-puckering states in the ground vibrational state $|0, n\rangle$ and in the first excited stretching state $|1, n\rangle$. The intensity of these transitions is given by

$$I_{|1,m\rangle\leftarrow|0,n\rangle} = \nu_{1m,0n}P\left(\int \Psi_{1m}^{*}(x)\left\langle 0\left|\frac{\partial\vec{\mu}(x)}{\partial r}r\right|1\right\rangle\Psi_{0n}(x)\,dx\right)^2 \quad (4)$$

where $\nu_{1m,0n}$ is the wavenumber of the transition ($(E_m^1 - E_n^0)/hc$), P is the Boltzmann factor, $\langle 1|$ and $|0\rangle$ are the vibrational wave functions corresponding to the first excited and the ground vibrational states, and r the C−H stretching coordinate. $(\partial\vec{\mu}(x)/\partial r)$ is the variation of the molecular dipole moment along x. This dipole moment has three Cartesian components along the main molecular axes X, Y, and Z (Figure 1A). The first derivative of these three components of the dipole moment can be determined from the ab initio computed atomic polar tensors using the procedure described previously.[22]

Finally, the effect of the rotation of the entire molecule is taken into account by convoluting each transition by the theoretical asymmetrical top vibration−rotation profile corresponding to each component of the dipole moment variation.

4. Results and Discussion

Experimental IR and VCD Spectra of 1. The experimental IR and VCD spectra of **1** are shown in Figures 2−4. The IR spectrum, recorded at a resolution of 0.5 cm^{-1}, exhibits the characteristic vibration−rotation profiles of an asymmetrical top already observed for the other cyclopentene derivatives.[10,12,13] In the C−H stretching region (Figure 2), the absorption spectrum of **1** is very similar to that of the mixed gaseous $3h_1$-d_7-cyclopentene and $4h_1$-d_7-cyclopentene.[10b,c] The VCD spectrum

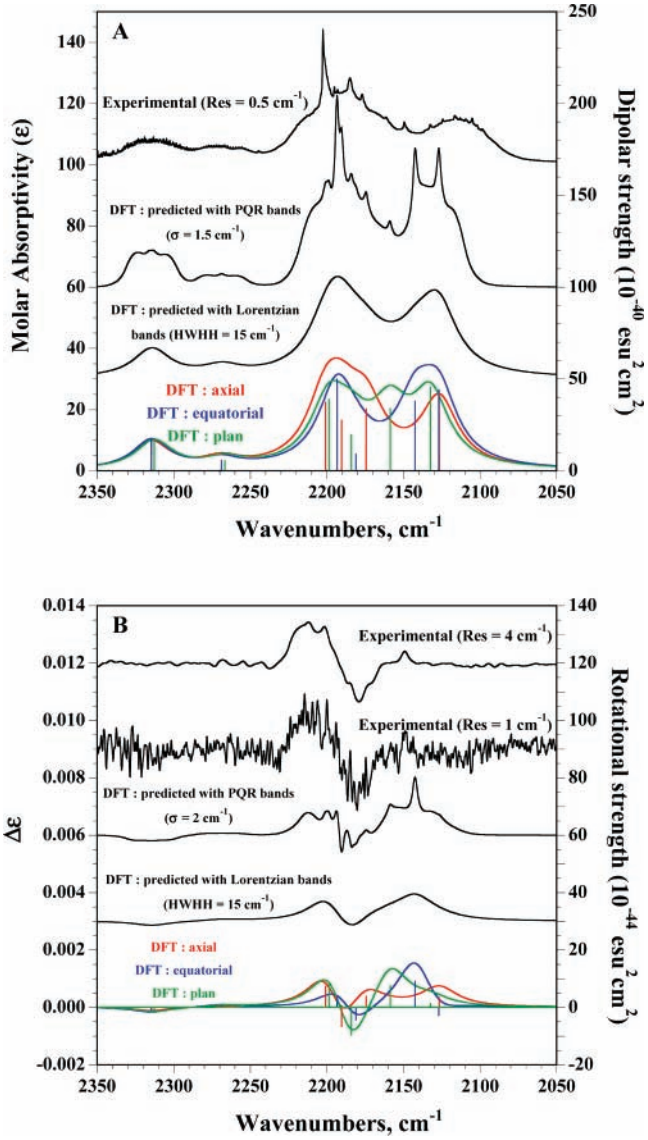

Figure 3. (A) Comparison of the experimental absorption spectrum of *trans*-(3*S*,4*S*)-d_6-cyclopentene in the gas phase (3.2 kPa, 100 mm path length, 0.5 cm^{-1} resolution; higher trace) with calculated absorption spectra in the 2350−2050 cm^{-1} region (lower trace, individual axial, equatorial, and planar conformer spectra; middle trace, predicted spectrum with Lorentzian profiles (15 cm^{-1} HWHH); upper trace, predicted spectrum with vibration−rotation PQR transitions convoluted with Lorentzian profile (1.5 cm^{-1} HWHH)). (B) Comparison of the experimental VCD spectra of *trans*-(3*S*,4*S*)-d_6-cyclopentene in the gas phase (3.2 kPa, 100 mm path length, 1 and 4 cm^{-1} resolution; higher traces) with calculated VCD spectra in the 2350−2050 cm^{-1} region (lower trace, individual axial, equatorial, and planar conformer spectra; middle trace, predicted spectrum with Lorentzian profiles (15 cm^{-1} HWHH); upper trace, predicted spectrum with vibration−rotation PQR transitions convoluted with Lorentzian profile (2 cm^{-1} HWHH)). The frequencies of the DFT spectra calculated at the B3LYP/cc-pVTZ level were scaled by 0.973.

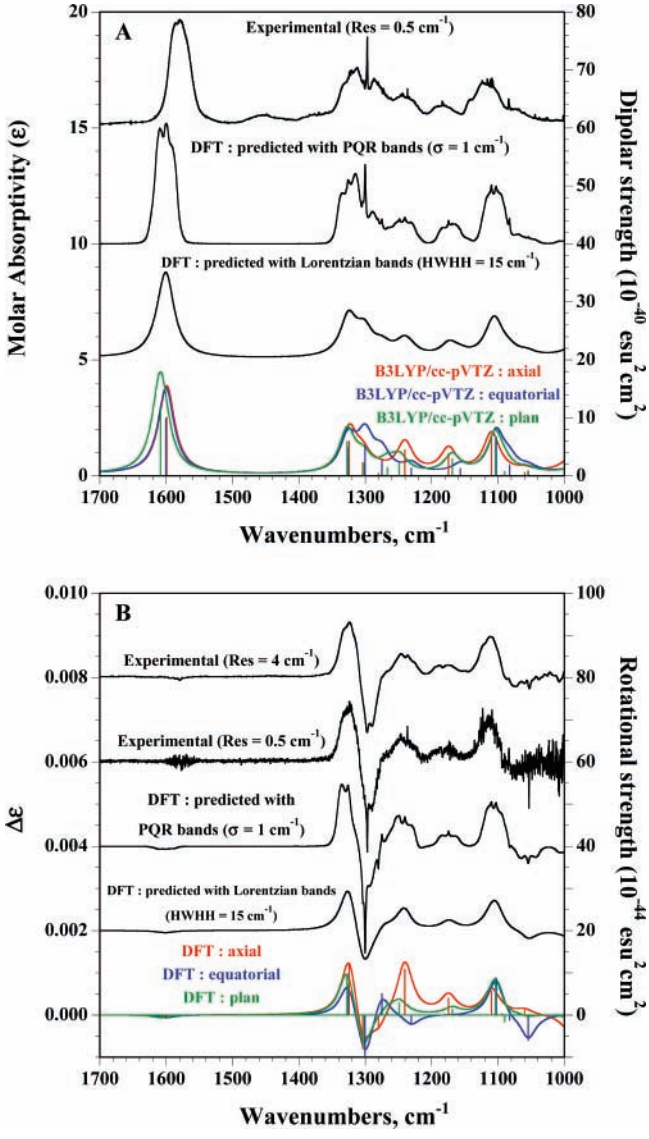

Figure 4. (A) Comparison of the experimental absorption spectrum of *trans*-(3*S*,4*S*)-d_6-cyclopentene in the gas phase (50.7 kPa, 100 mm path length, 0.5 cm^{-1} resolution; higher trace) with calculated absorption spectra in the 1700−1000 cm^{-1} region (lower trace, individual axial, equatorial, and planar conformer spectra; middle trace, predicted spectrum with Lorentzian profiles (15 cm^{-1} HWHH); upper trace, predicted spectrum with vibration−rotation PQR transitions convoluted with Lorentzian profile (1 cm^{-1} HWHH)). (B) Comparison of the experimental VCD spectra of *trans*-(3*S*,4*S*)-d_6-cyclopentene in the gas phase (50.7 kPa, 100 mm path length, 0.5 and 4 cm^{-1} resolution; higher traces) with calculated VCD spectra in the 1700−1000 cm^{-1} region (lower trace, individual axial, equatorial, and planar conformer spectra; middle trace, predicted spectrum with Lorentzian profiles (15 cm^{-1} HWHH); upper trace, predicted spectrum with vibration−rotation PQR transitions convoluted with Lorentzian profile (1 cm^{-1} HWHH)). The frequencies of the DFT spectra calculated at the B3LYP/cc-pVTZ level were scaled by 0.98.

below 2000 cm^{-1} was also recorded at a resolution of 0.5 cm^{-1}. This VCD spectrum is the first gas-phase VCD at this resolution to be reported. The VCD spectra in the C−H and C−D stretching regions were recorded at a resolution of 1 cm^{-1}. A lower resolution had been used to improve the signal-to-noise ratio (S/N) of the VCD spectra. This S/N deterioration comes from the lack of efficient optical filter in these spectral ranges and the decrease of interferometer stability at low wavelength. As previously noted for *trans*-(1*S*,2*S*)-dideuteriocyclopropane,[5] the VCD spectra recorded at high resolution (0.5 cm^{-1} and 1 cm^{-1}) show the same contours as the absorption bands for all the modes. These features, even less resolved, are still observable in the VCD spectra recorded at a resolution of 4 cm^{-1}. However, the S/N ratio was considerably higher at this lower resolution.

Conformational Analysis of 1. The geometries of the two puckered conformations (i.e., axial and equatorial as shown in Figure 1B) of **1** were optimized at the B3LYP/cc-pVTZ level. Harmonic vibrational frequencies have been calculated at the same level to confirm that the two structures are stable

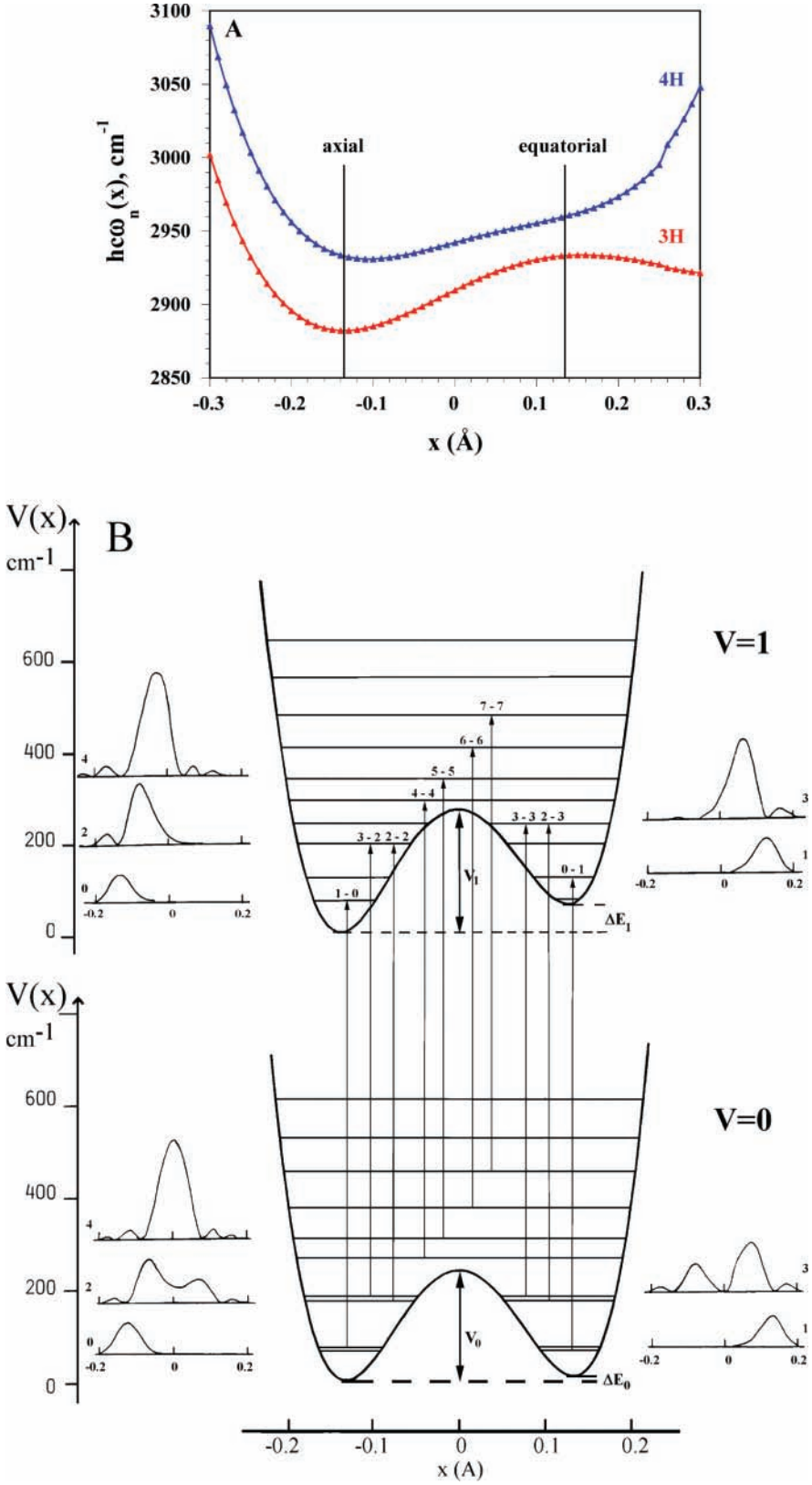

Figure 5. (A) Calculated vibrational energy variation $hc\omega_n(x)$ of each C−H stretching mode with respect to the ring-puckering motion. (B) Calculated effective potentials of the ring-puckering motion in the ground and in the first excited $C_{(3)}H_{(8)}$ stretching vibrational state. The most intense transitions are indicated by arrows, and the square wave functions of the first ring-puckering levels are drawn for each vibrational state to show the localization in each potential well.

conformations and to enable free energies to be calculated. The constrained planar conformer which corresponds to a transition state was also calculated to estimate the potential barrier height and to check its eventual contribution to the spectral features. The converged electronic and Gibbs energies are listed in Table 1. The two equilibrium puckered conformations are of similar energy ($\Delta E_{a-e} = 3.3$ cm^{-1}) with a calculated puckering angle $\theta = 19.6°$. The value of the calculated potential barrier height, given by the energy difference with the plane conformation ΔE_{a-p}, is equal to 223.2 cm^{-1}. Even if this value is relatively

TABLE 2: Variation along the Ring-Puckering Coordinate *x* (in Å) of the Parameters Used To Model the C−H Stretching Absorption Spectrum

	$C_{(3)}H_{(8)}$ stretching	$C_{(4)}H_{(10)}$ stretching
$hc\omega_0(x)^a$	$3038.6 + 273x + 109x^2 - 4732x^3 - 3389x^4 + 4369x^5 + 111150x^6$	$2973.5 + 135x - 338x^2 - 2208x^3 + 21000x^4$
$\chi(x)^b$	$64.6 - 2.5x - 34.5x^2 - 44.5x^3 + 1250x^4$	$62.6 - 5.5x - 69.5x^2 - 89.0x^3 + 2500x^4$
$\mu_X(x)^c$	$0.2017 - 0.2701x - 0.429x^2$	0
$\mu_Y(x)^c$	$0.0433 - 0.0715x + 0.228x^2$	$0.1812 - 0.4641x + 0.342x^2$
$\mu_Z(x)^c$	$0.1822 + 0.3584x - 0.837x^2$	$-0.1514 - 0.4199x + 0.040x^2$
$g(x)^d$	$6.1571 \times 10^{-3} - 2.1109 \times 10^{-5}x - 6.96951 \times 10^{-3}x^2 - 2.9721 \times 10^{-3}x^3 - 2.2066 \times 10^{-1}x^4 - 2.1145 \times 10^{-2}x^5 - 8.9568 \times 10^{-1}x^6$	
$V^0_{\text{eff}}(x)^e$	$-26452x^2 + 952.8x^3 - 754020x^4$	

[a] Harmonic frequency in cm^{-1}. For the fundamental C−H stretching: $hc\omega_n(x) = hc\omega_0(x) - 2\chi(x)$. [b] Anharmonicity in cm^{-1}. [c] Components of the dipole moment $\partial\vec{\mu}(x)/\partial r$ in debye $Å^{-1}$. [d] Inverse of the reduced mass of the ring-puckering motion. [e] Ring-puckering potential in the fundamental state in cm^{-1}.

high, the population of the planar conformer cannot be neglected in the following.

Calculated IR and VCD Spectra of 1. The frequencies and dipolar and rotational strengths of the 3*N*-6 (i.e., 33) vibrations, calculated at the B3LYP/cc-pVTZ level for individual conformers, are given in the Supporting Information. The proportion (%) of "A", "B", and "C type" contours for each mode is also reported.

The calculated IR and VCD spectra are shown in Figure 2 in the C−H stretching region. DFT calculations predict a higher C−H stretching vibration for the $C_{(4)}H_{(10)}$ bond with respect to the $C_{(3)}H_{(8)}$ bond, whatever the conformer. Moreover, for a given C−H bond, the axial conformer is calculated at a lower frequency. These features are mainly due to hyper-conjugation effects induced by the C═C bond. As observed in Figure 2, the IR spectra of individual conformer, modeled with Lorentzian profile, overlap in the C−H stretching region. The predicted absorption spectrum is represented by a broad profile formed from the population-weighted sum of the contribution of the axial, equatorial, and planar conformers. It reproduces fairly well the overall spectral feature of the experimental spectrum. However, to take into account the observed vibration−rotation structure, the absorption spectrum has been predicted using PQR profile. This calculated spectrum exhibits the major patterns seen in the experimental one: Q branches with high and medium intensities for the $C_{(4)}H_{(10)}$ and $C_{(3)}H_{(8)}$ stretching vibrations of the axial conformer, respectively, and Q branch with low intensity for the $C_{(4)}H_{(10)}$ stretching vibration of the equatorial conformer. On the other hand, the calculated frequencies of the $C_{(3)}H_{(8)}$ stretching vibration of the equatorial conformer and that of the $C_{(4)}H_{(10)}$ stretching vibration of the axial conformer are split by 15 cm^{-1}, whereas these two modes are observed at the same frequency in the experimental spectrum. Moreover, the pattern observed close to 2945 cm^{-1} in the experimental spectrum is not reproduced in the predicted spectrum. To cancel this disagreement, the coupling of the C−H stretching with the ring-puckering motion as well as anharmonicity of the C−H stretching vibration should be taken into account (vide infra).

Concerning VCD, the rotational strength associated to the $C_{(3)}H_{(8)}$ stretching vibration is calculated negative for the three conformers whereas it is calculated positive for the $C_{(4)}H_{(10)}$ stretching vibration. This feature gives rise to a (+,−) VCD sign pattern in the C−H stretching region. This derivative shape could be interpreted using the degenerate coupled oscillator (DCO) model.[23] This coupling occurs between all pairs of local oscillators and can produce significant VCD when the transition dipole moments are large and the involved modes are strongly coupled.[24] Moreover, the hypothesis of coupled dipoles for a chiral HCCH fragment has been suggested in a recent article.[25] However, when considering the DCO model, in-phase and out-of-phase C−H stretching modes are expected. This coupling has not been evidenced in our DFT calculations because the contributions to the potential energy distribution (PED) are close to 100% for the two localized C−H stretching modes (see Supporting Information). Thus, VCD intensity of **1** must derive essentially from intrinsic magnetic dipole moment effects. The predicted VCD spectrum with PQR profile matches well the experimental spectrum recorded at a resolution of 1 cm^{-1}, in particular the positive and negative Q branches for the $C_{(4)}H_{(10)}$ and $C_{(3)}H_{(8)}$ stretching vibrations of the axial conformer, respectively. The good agreement between theoretical and experimental IR and VCD spectra in the C−H stretching region is mainly due to the fact that no Fermi resonance occurs in this spectral range. Finally, it is noteworthy that the contribution (i.e., 14%) of the planar conformer improves this agreement.

The calculated IR and VCD spectra of **1** are shown in Figure 3 in the C−D stretching region. The two higher frequency bands at 2308 and 2263 cm^{-1} are assigned to asymmetric (ν_{as}) and symmetric (ν_s) stretching of the ethylenic $C_{(1)}D_{(6)}$ and $C_{(2)}D_{(7)}$ bonds. Their optical activity is very low, with a negative and positive sign for ν_{as} and ν_s vibrations, respectively, whatever the puckered conformation. The pattern of the other C−D stretching vibrations is more complex. If the symmetric stretching vibration ν_sCD_2 of the $C_{(5)}D_{(12)}D_{(13)}$ group is pure for the three conformers, this is not the case of the asymmetric mode $\nu_{as}CD_2$. Indeed, it mixes with the adjacent $C_{(4)}D_{(11)}$ stretching vibration in the equatorial conformer. Furthermore, Fermi resonance phenomena cannot be disregarded in this region. Nevertheless, the general features of the predicted absorption spectrum are in reasonable agreement with the experimental ones. Indeed, the predicted IR spectrum calculated with Lorentzian profile reproduces the overall spectral feature of the experimental spectrum. However, when IR spectrum is calculated with PQR profile some discrepancies appear, in particular in the 2150−2100 cm^{-1} region where two Q branches with medium intensity are calculated at 2137 and 2122 cm^{-1} but not observed. They correspond to the Q branches of the "AC type" $\nu C_{(3)}D_{(9)}$ mode of the equatorial conformer and to the "A type" ν_sCD_2 mode of the axial and equatorial conformers which have similar frequency, respectively. This last difference disappears in the predicted VCD spectrum because the two ν_sCD_2 bands have similar but inverse rotational strengths and cancel each other. Finally, the predicted VCD spectrum with PQR profile is in fairly good agreement with the experimental one recorded at a resolution of 4 cm^{-1}.

The calculated IR and VCD spectra of **1** are shown in Figure 4 in the mid-IR region. The higher frequency band at 1576 cm^{-1} is assigned to the ethylenic C═C stretching vibration. The calculated frequency of this "B type" band is rather independent of the molecular conformation. This mode presents a very low negative optical activity as experimentally observed. The rather strong VCD bands observed at 1325 and 1300 cm^{-1} correspond

to the in-phase and out-of-phase bending modes of the $C_{(3)}H_{(8)}D_{(9)}$ and $C_{(4)}H_{(10)}D_{(11)}$ groups, respectively. Their frequencies are also rather independent of the molecular conformation. Main "B" and "C type" vibration−rotation structures are calculated for these two modes, respectively. The high anisotropy ratio ($g = 4R/D$) calculated for these two modes (close to $\pm 1 \times 10^{-3}$) comes certainly from a coupled-oscillator mechanism as suggesting by the coupling of the CHD bending vibration. The bands observed at 1236 cm^{-1} can be mainly associated to the $CC_{(3)}H_{(8)}$ bending mode of the axial conformer whereas the assignment of bands located at 1183, 1123, and 1086 cm^{-1} is less straightforward because different motions are involved in these modes. The predicted IR and VCD spectra with Lorentzian profile match very well the overall features observed in the experimental ones. Moreover, when the PQR profile is used, the Q branch intensities are perfectly reproduced for the different modes. This very good agreement between theoretical and experimental spectra comes from the fact that anharmonicity and Fermi resonance effects as well as coupling of the modes with the ring-puckering motion have minor contributions in this spectral range. Moreover, as this study has been performed in the gas phase, a direct comparison of the DFT calculations can be made with experiments (no intermolecular interaction with a solvent).

Calculated IR Spectrum of 1 with Coupling of the C−H Stretching with the Ring-Puckering Motion. A better reproduction of the absorption spectrum in the C−H stretching region can only been achieved by considering the coupling of these vibrations with the puckering motion.[10b,c,12,13] Thus, we have calculated the absorption spectrum in this region with the theoretical model recalled above. In the present study, the local parameters for the C−H bond stretching modes (harmonic frequency $hc\omega_0$ and anharmonicity χ), the three components of their dipole moment, the harmonic interaction parameters, and the parameters related to the couplings between the C−H stretching and the deformation modes attached to the same carbon atom (C_3 or C_4) as well as their variation along the puckering coordinate x have been determined in previous studies.[13] The variation along x of the main used parameters is reported in Table 2. Calculation of the adiabatic vibrational energy variations, $hc\omega_n(x)$, evidence that both C−H stretching modes are not perturbed by Fermi resonance. These variations are displayed in Figure 5A. In the ground vibrational state, zero point vibrational energy gives an asymmetrical character to the ring-puckering potential, the C−H axial conformation being slightly more stable than the equatorial one (Figure 5B). In the first excited vibrational state, the additional vibrational energy variation $hc\omega_n(x)$ increases this asymmetry. This asymmetry leads to a strong localization of the wave functions in each potential well of the two first ring-puckering levels in both ground and first excited vibrational C−H stretching state (Figure 5B). Consequently, only few $|0, n\rangle \rightarrow |1, n\rangle$ fundamental C−H stretching transitions have significant intensity. The most intense transitions are plotted as sticks in Figure 6, and their intensities along the X, Y, and Z axes are listed in Table 3. For the $C_{(3)}H_{(8)}$ stretching, the component μ_Y has a very weak value compared to the two other ones whereas the component μ_X is equal to zero for $C_{(4)}H_{(10)}$ stretching. Thus, the rotation−vibration contours of these vibrations are essentially of "A, C type" and of "B, C type", respectively, as above observed in the Gaussian calculations. The $|0, 1\rangle \rightarrow |1, 0\rangle$ transitions give rise to the two bands with a predominant "C type" contour observed at 2884.3 and 2933.2 cm^{-1} corresponding to the axial conformation of the $C_{(3)}H_{(8)}$ and $C_{(4)}H_{(10)}$ bonds, respectively. The $|0, 0\rangle \rightarrow |1, 1\rangle$ transitions give rise to a band with a predominant "A type" contour at 2932.0 cm^{-1} and to a band with a predominant "B type" contour at 2958.2 cm^{-1} corresponding to the equatorial conformation of the $C_{(3)}H_{(8)}$ and $C_{(4)}H_{(10)}$ bonds, respectively. The $|0, n\rangle \rightarrow |1, n\rangle$ transitions with $n \geq 4$ give rise to weaker bands at a frequency around 2910 and 2948 cm^{-1} for the $C_{(3)}H_{(8)}$ and $C_{(4)}H_{(10)}$ bonds, respectively. These last transitions, issued from puckering levels with higher energy than the puckering barrier height, correspond to the planar conformation of the molecule. The transitions with $1 < n < 4$ involving puckering levels with lower energy than the puckering barrier height give rise to all the other spectral features observed in the experimental spectrum. As shown in Figure 6, a better agreement between experimental and calculated IR spectra is obtained when anharmonicity and coupling of the C−H stretching with the ring-puckering motion are considered.

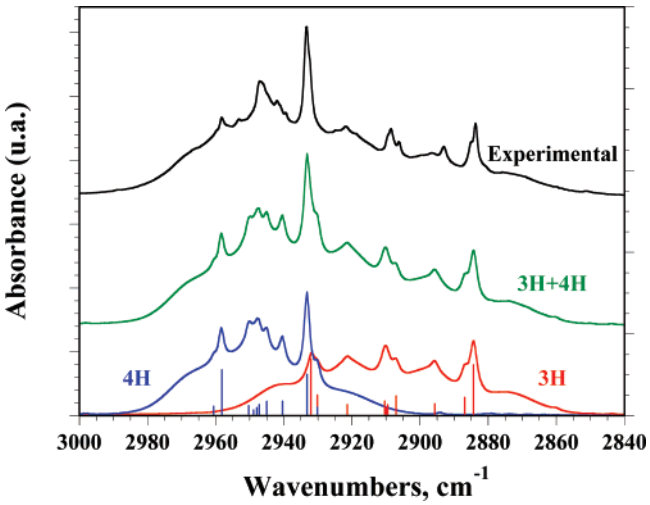

Figure 6. Comparison of the C−H stretching experimental absorption spectrum of *trans*-(3*S*,4*S*)-d_6-cyclopentene in the gas phase (3.2 kPa, 100 mm path length, 0.5 cm^{-1} resolution; higher trace) with absorption spectra predicted by using the model taking into account the coupling with the ring-puckering motion (lower trace, individual $C_{(3)}H_{(8)}$ and $C_{(4)}H_{(10)}$ stretching spectra; middle trace, sum of the two spectra). The calculated spectra were simulated with vibration−rotation PQR transitions convoluted with Lorentzian profile (1.5 cm^{-1} HWHH).

TABLE 3: Principal Calculated $|0, n\rangle \rightarrow |1, n\rangle$ Fundamental C−H Stretching Transitions[a]

	$C_{(3)}H_{(8)}$ stretching				$C_{(4)}H_{(10)}$ stretching			
transition	ν^b	$I_X{}^c$	$I_Y{}^c$	$I_Z{}^c$	ν^b	$I_X{}^c$	$I_Y{}^c$	$I_Z{}^c$
$\|0, 1\rangle \rightarrow \|1, 0\rangle$	2884.3	0.415	0.043	0.789	2933.2	0	0.190	0.823
$\|0, 0\rangle \rightarrow \|1, 1\rangle$	2932.0	1.0	0.001	0.390	2958.2	0	1.0	0.119
$\|0, 3\rangle \rightarrow \|1, 2\rangle$	2886.9	0.156	0.016	0.277	2930.1	0	0.022	0.178
$\|0, 2\rangle \rightarrow \|1, 3\rangle$	2930.1	0.347	0.001	0.159	2960. 6	0	0.215	0.013
$\|0, 2\rangle \rightarrow \|1, 2\rangle$	2895.7	0.118	0.007	0.164	2940.4	0	0.142	0.213
$\|0, 3\rangle \rightarrow \|1, 3\rangle$	2921.4	0.173	0.001	0.100	2950.3	0	0.243	0.104
$\|0, 4\rangle \rightarrow \|1, 4\rangle$	2907.0	0.238	0.009	0.237	2945.0	0	0.186	0.160
$\|0, 5\rangle \rightarrow \|1, 5\rangle$	2910.4	0.194	0.005	0.164	2947.2	0	0.154	0.119
$\|0, 6\rangle \rightarrow \|1, 6\rangle$	2909.5	0.144	0.004	0.125	2947.9	0	0.111	0.088
$\|0, 7\rangle \rightarrow \|1, 7\rangle$	2909.9	0.102	0.003	0.087	2948.9	0	0.078	0.062

[a] 0, 1: Stretching vibrational state. n: Ring-puckering vibration levels. [b] Frequency in cm^{-1}. [c] Transition intensity; the values are normalized with respect to the strongest component one.

5. Conclusion

In this study, we have shown that VCD spectra of *trans*-(3*S*,4*S*)-d_6-cyclopentene in the gas phase can be recorded at high spectral resolution (up to 0.5 cm^{-1}) with a very good signal-to-noise ratio. This high spectral resolution was necessary to

define precisely the vibration−rotation structure of the bands. We have also documented the accuracy of DFT (B3LYP functional and cc-pVTZ basis set) in predicting the vibrational frequencies as well as the absorption and VCD intensities of the axial, equatorial, and planar conformers of *trans*-(3*S*,4*S*)-d_6-cyclopentene. To improve the comparison with the experimental spectra recorded at high spectral resolution, the predicted (population-weighted) IR and VCD spectra have been calculated using PQR band profile. In the mid-IR region, our harmonic calculations are in excellent agreement with experiment, allowing the determination of the absolute configuration of this molecule. For the C−D stretching modes, due to Fermi resonance perturbation, the correspondence of theory and experiment is less good, in particular for the absorption spectrum. For the C−H stretching modes, a reasonable agreement with experiment is obtained even if their vibrational frequencies are not perfectly predicted due to anharmonicity effect. A more precise analysis of the absorption spectrum has been achieved by taking into account this effect and the coupling of the C−H stretching with the ring-puckering motion.

Acknowledgment. We are indebted to the CNRS (Chemistry Department) and to Région Aquitaine for financial support in FTIR and optical equipment. We gratefully acknowledge the Mesocentre Régional de Calcul en Aquitaine (M3PEC-MRCA) for allocating computing time and providing facilities. We also thank very much M. F. Lautié for the synthesis of *trans*-(3*S*,4*S*)-d_6-cyclopentene and S. Abbate of the University of Brescia for very helpful discussions which have initiated the synthesis of **1**.

Supporting Information Available: Predicted frequencies, dipolar strength, rotational strength, ratio (%) of "A", "B", and "C type" vibration−rotation profiles, and assignment of the axial, equatorial, and planar conformers of **1**. This material is available free of charge via the Internet at http://pubs.acs.org.

References and Notes

(1) Nafie, L. A.; Dukor, R. K.; Freedman, T. B. In *Handbook of Vibrational Spectroscopy*; Chalmers, J. M., Griffiths, P. R., Eds.; John Wiley & Sons: Chichester, 2002; Vol. 1, pp 731−744.

(2) Freedman, T. B.; Cao, X.; Dukor, R. K.; Nafie, L. A. *Chirality* **2003**, *15*, 743−758 and references therein.

(3) Stephens, P. J.; Devlin, F. J. *Chirality* **2000**, *12*, 172−179 and references therein.

(4) (a) Annamalaï, A.; Kiederling, T. A.; Chickos, J. S. *J. Am. Chem. Soc.* **1984**, *106*, 6254−6265; *J. Am. Chem. Soc.* **1985**, *107*, 2285−2291. (b) Annamalaï, A.; Kiederling, T. A. *J. Mol. Spectrosc.* **1985**, *109*, 46.

(5) Cianciosi, S. J.; Spencer, K. M.; Freedman, T. B.; Nafie, L. A.; Baldwin, J. E. *J. Am. Chem. Soc.* **1989**, *111*, 1913−1915.

(6) (a) Freedman, T. B.; Cianciosi, S. J.; Ragunathan, N.; Baldwin, J. E.; Nafie, L. A. *J. Am. Chem. Soc.* **1991**, *113*, 8298−8305. (b) Freedman, T. B.; Hausch, D. L.; Cianciosi, S. J.; Baldwin, J. E. *Can. J. Chem.* **1998**, *76*, 806−810.

(7) (a) Schellman, J. A. *J. Chem. Phys.* **1973**, *58*, 2882. (b) Schellman, J. A *J. Chem. Phys.* **1974**, *60*, 343.

(8) (a) Nafie, L. A.; Walnut, T. H. *Chem. Phys. Lett.* **1977**, *49*, 441. (b) Walnut, T. H.; Nafie, L. A. *J. Chem. Phys.* **1977**, *67*, 1501. (c) Nafie, L. A.; Polavarapu, P. L. J. *Chem. Phys.* **1981**, *75*, 2935. (d) Polavarapu, P. L.; Nafie, L. A. J. *Chem. Phys.* **1981**, *75*, 2945.

(9) (a) Rathjens, G. W. *J. Chem. Phys.* **1962**, *36*, 2401. (b) Butcher, S. S.; Costain, C. C. *J. Mol. Spectrosc.* **1965**, *15*, 40. (c) Laane, J.; Lord, R. C. *J. Chem. Phys.* **1967**, *47*, 4941. (d) Ueda, T.; Shimanouchi, T. *J. Chem. Phys.* **1967**, *47*, 5018. (e) Green, W. H. *J. Chem. Phys.* **1970**, *52*, 2156. (f) Davis, M. I. Muecke, J. W. *J. Phys. Chem.* **1970**, *74*, 1104. (g) Durig, J. R.; Carreira, L. A. *J. Chem. Phys.* **1972**, *56*, 4966. (h) Lopez, J. C.; Alonso, J. L.; Charro, M. E.; Wlodarczak, G.; Demaison, J. *J. Mol. Spectrosc.* **1992**, *143*, 1555. (i) Villareal, J. R.; Bauman, L. E.; Laane, J.; Harris, W. C.; Bush, S. F. *J. Chem. Phys.* **1975**, *63*, 3727. (j) Villareal, J. R.; Bauman, L. E.; Laane, J. *J. Phys. Chem.* **1976**, *80*, 1172. (k) Villareal, J. R.; Laane, J.; Bush, S. F.; Harris, W. C. *Spectrochim. Acta, Part A* **1979**, *35A*, 331. (l) Bauman, L. E.; Killough, P. M.; Cooke, J. M.; Villareal, J. R.; Laane, J. *J. Phys. Chem.* **1982**, *86*, 2000.

(10) (a) Cavagnat, D.; Banisaeid-Vahedie, S.; Grignon-Dubois, M. *J. Phys. Chem.* **1991**, *95*, 5073. (b) Cavagnat, D.; Banisaed-Vahedie, S. *J. Phys. Chem.* **1991**, *95*, 8529. (c) Cavagnat, D.; Banisaeid-Vahedie, S.; Lespade, L.; Rodin, S. *J. Chem. Soc., Faraday Trans.* **1992**, *88*, 1845.

(11) (a) Rathjens, G. W. *J. Chem. Phys.* **1962**, *36*, 2401. (b) Scharpen, L. H. *J. Chem. Phys.* **1968**, *48*, 3552. (c) Malloy, T. B. *J. Mol. Spectrosc.* **1972**, *44*, 504. (d) De Alti, G.; Decleva, P. *J. Mol. Struct.* **1977**, *41*, 299. (e) Malloy, T. B.; Carreira, L. A. *J. Chem. Phys.* **1979**, *71*, 2488. (f) Saebø, S.; Cordell, F. R. Boggs. J. *J. Mol. Struct.* **1983**, *104*, 221. (g) Champion, R.; Godfrey, P. D.; Bettens, F. L. *J. Mol. Struct.* **1991**, *147*, 488. (h) Pyka, J. *J. Mol. Spectrosc.* **1992**, *151*, 423. (i) Sztraka, L. *Spectrochim. Acta* **1992**, *48A*, 65. (j) Allen, W. D.; Csaszar, A. G.; Horner, D. A. *J. Am. Chem. Soc.* **1992**, *114*, 6834.

(12) (a) Lapouge, C.; Cavagnat, D.; Gorse, D.; Pesquer, M. *J. Phys. Chem.* **1995**, *99*, 2996. (b) Rodin-Bercion, S.; Cavagnat, D.; Lespade, L.; Maraval, P. *J. Phys. Chem.* **1995**, *99*, 3005. (c) Lespade, L.; Rodin-Bercion, S.; Cavagnat, D. *J. Phys. Chem. A* **1997**, *101*, 2568. (d) Lespade, L.; Rodin-Bercion, S.; Cavagnat, D. *J. Phys. Chem. A* **2000**, *104*, 9880.

(13) (a) Lespade, L.; Cavagnat, D.; Asselin, P. *J. Phys. Chem. A* **2002**, *106*, 9451. (b) Cavagnat, D.; Lespade, L.; Lacome, N. *J. Phys. Chem. A* **2002**, *106*, 9460.

(14) Chickos, J. S.; Bausch, M.; Alul, R. *J. Org. Chem.* **1981**, *46*, 3559.

(15) Lautie, M. F. Private communication.

(16) Buffeteau, T.; Lagugné-Labarthet, F.; Sourisseau, C. *Appl. Spectrosc.* **2005**, *59*, 732−745.

(17) Nafie, L. A.; Vidrine, D. W. In *Fourier Transform Spectroscopy*; Ferraro, J. R., Basile, L. J., Eds.; Academic Press: New York, 1982; Vol. 3, pp 83−123.

(18) Frisch, M. J.; Trucks, G. W.; Schlegel, H. B.; Scuseria, G. E.; Robb, M. A.; Cheeseman, J. R.; Montgomery, J. A., Jr.; Vreven, T.; Kudin, K. N.; Burant, J. C.; Millam, J. M.; Iyengar, S. S.; Tomasi, J.; Barone, V.; Mennucci, B.; Cossi, M.; Scalmani, G.; Rega, N.; Petersson, G. A.; Nakatsuji, H.; Hada, M.; Ehara, M.; Toyota, K.; Fukuda, R.; Hasegawa, J.; Ishida, M.; Nakajima, T.; Honda, Y.; Kitao, O.; Nakai, H.; Klene, M.; Li, X.; Knox, J. E.; Hratchian, H. P.; Cross, J. B.; Bakken, V.; Adamo, C.; Jaramillo, J.; Gomperts, R.; Stratmann, R. E.; Yazyev, O.; Austin, A. J.; Cammi, R.; Pomelli, C.; Ochterski, J. W.; Ayala, P. Y.; Morokuma, K.; Voth, G. A.; Salvador, P.; Dannenberg, J. J.; Zakrzewski, V. G.; Dapprich, S.; Daniels, A. D.; Strain, M. C.; Farkas, O.; Malick, D. K.; Rabuck, A. D.; Raghavachari, K.; Foresman, J. B.; Ortiz, J. V.; Cui, Q.; Baboul, A. G.; Clifford, S.; Cioslowski, J.; Stefanov, B. B.; Liu, G.; Liashenko, A.; Piskorz, P.; Komaromi, I.; Martin, R. L.; Fox, D. J.; Keith, T.; Al-Laham, M. A.; Peng, C. Y.; Nanayakkara, A.; Challacombe, M.; Gill, P. M. W.; Johnson, B.; Chen, W.; Wong, M. W.; Gonzalez, C.; Pople, J. A. *Gaussian 03*, revision B.04; Gaussian, Inc.: Wallingford, CT, 2004.

(19) Cheesemann, J. R.; Frisch, M. J.; Delvin, F. J.; Stephens, P. J. J. *Chem. Phys. Lett.* **1996**, *252*, 211−220.

(20) Herzberg, G. *Molecular Spectra and Molecular Structure. II Infrared and raman Polyatomic Molecules*, D. Van Nostrand Company, Inc.: Princeton, NJ, 1956; Chapter IV.4, pp 460−491.

(21) Perrin, A. Private communication

(22) (a) Biarge, J. F.; Herrantz, J.; Morcillo, J. *J. Annu. Rev. Soc. Esp. Fis. Quim.* **1961**, *A57*, 81. (b) Person, W. B.; Newton, J. H. *J. Chem. Phys.* **1974**, *61*, 1040.

(23) (a) Holzwarth, G.; Chabay, I. *J. Chem. Phys.***1972**, *57*, 1632. (b) Tinoco, I. *Radiat. Res.* **1963**, *20*, 133.

(24) (a) Narayanan, U.; Keiderling, T. A. *J. Am. Chem. Soc.* **1983**, *105*, 6406. (b) Su.; C. N.; Keiderling, T. A. *J. Am. Chem. Soc.* **1980**, *102*, 511.

(25) Gangemi, R.; Longhi, G.; Abbate, S. *Chirality* **2005**, *17*, 530.